HHS Public Access

Author manuscript

J Hepatol. Author manuscript; available in PMC 2016 April 01.

Published in final edited form as:

J Hepatol. 2015 April ; 62(4): 879–888. doi:10.1016/j.jhep.2014.11.010.

Endoplasmic reticulum heat shock protein gp96 maintains liver homeostasis and promotes hepatocellular carcinogenesis

Saleh Rachidi[1,2], **Shaoli Sun**[3], **Bill X Wu**[1,2], **Elizabeth Jones**[4], **Richard R. Drake**[4], **Besim Ogretmen**[5], **Ashley Cowart**[5,6], **Christopher J. Clarke**[7], **Yusuf A. Hannun**[7], **Gabriela Chiosis**[8], **Bei Liu**[1,2], and **Zihai Li**[1,2,*]

[1]Department of Microbiology and Immunology, Medical University of South Carolina, Charleston, SC

[2]Hollings Cancer Center, Medical University of South Carolina, Charleston, SC

[3]Department of Pathology, Medical University of South Carolina, Charleston, SC

[4]Department of Cell and Molecular Pharmacology, Medical University of South Carolina, Charleston, SC

[5]Department of Biochemistry and Molecular Biology, Medical University of South Carolina, Charleston, SC

[6]Ralph H. Johnson Veteran's Affairs Medical Center, Charleston, SC

[7]Department of Medicine, Stony Brook University, Stony Brook, New York

[8]Program in Molecular Pharmacology and Chemistry, Memorial Sloan-Kettering Cancer Center, New York, NY

Abstract

Background & Aims—gp96, or grp94, is an endoplasmic reticulum (ER) heat shock protein 90 paralog which acts as a protein chaperone and plays an important role in ER homeostasis. Previous work has demonstrated its role in ER stress, Wnt and integrin signaling, calcium homeostasis and others, which are vital processes in oncogenesis. However, the cancer-intrinsic function of gp96 remains controversial.

Methods—We studied the roles of gp96 in liver biology in mice via an *albumin* promoter-driven cre recombinase-mediated disruption of gp96 gene, *hsp90b1*. The impact of gp96 status on hepatic carcinogenesis in response to diethyl-nitrosoamine (DENA) was probed. The roles of gp96 on

*Corresponding author. Tel: 843-792-1034; Fax: 843-792-9588; zihai@musc.edu.

Conflict of interests: none

Author's contributions: experimental design and performance (SR, SS, BXW, EJ, RRD, CJC), provider of critical reagents (GC), discussion and data interpretation (BO, AC, YAH, BL), writing of the manuscript (SR and ZL), project supervision (ZL).

human hepatocellular carcinoma cells (HCC) were also examined pharmacologically with a targeted gp96 inhibitor.

Results—We demonstrated that gp96 maintains liver development and hepatocyte function *in vivo*, and its loss genetically promotes adaptive accumulation of long chain ceramides, accompanied by steatotic regeneration of residual gp96+ hepatocytes. The need for compensatory expansion of gp96+ cells in the gp96− background predisposes mice to develop carcinogen-induced hepatic hyperplasia and cancer from gp96+ but not gp96− hepatocytes. We also found that genetic and pharmacological inhibition of gp96 in human HCCs perturbs multiple growth signals, and attenuates their proliferation and expansion.

Conclusions—gp96 is a pro-oncogenic chaperone, and is an attractive therapeutic target for HCC.

Keywords

grp94; molecular chaperone; liver cancer; gp96

Introduction

gp96 (also called grp94, endoplasmin, ERp99 or HSP90B1) is an endoplasmic reticulum (ER) paralog of the cytosolic heat shock protein 90 (HSP90). It chaperones and aids in the folding of client proteins including Toll-like receptors (1–3), Wnt co-receptor LRP6 (4), insulin-like growth factors (5) and integrins (6–8). gp96 is also induced under glucose starvation and other stress conditions (9). Along with grp78, gp96 is an effector molecule of the unfolded protein response (UPR) in the ER lumen (10, 11). As an adaptive mechanism tailored to cope with the increased burden of misfolded proteins, UPR is initiated through three well-characterized and evolutionally conserved UPR sensors including the double-stranded RNA-activated protein kinase-like ER kinase (PERK), activating transcription factor 6 (ATF6), and the spliced form of X box binding protein 1 (XBP1s) (12–16). The three UPR pathways are ultimately responsible for alleviating ER stress by attenuating further translation, increasing ER chaperone machinery and maintaining proper protein quality control in the secretory pathway. As such, gp96 is an integral component of the ER homeostatic machinery and its deletion is expected to result in a burden of misfolded proteins, inducing UPR and ultimately cell death if UPR fails to restore normal physiologic ER function.

The liver is an exocrine and endocrine organ involved in synthesizing a myriad of bioactive molecules in normal and disease conditions, including albumin, coagulation factors, complement proteins, C-reactive protein and many others. In addition, hepatocytes are involved in the detoxification of physiological metabolites including ammonia, bilirubin and others as well as many xenobiotic substances. Their distinctive anatomical position allows them to receive blood draining the gastrointestinal tract through the portal vein, thus placing them strategically to detoxify absorbed non-physiological toxins. Therefore, hepatocytes are highly metabolic cells with active protein synthesis and secretory machinery, which necessitates adequate ER maintenance wiring and efficient stress-coping mechanisms. This suggests that loss of gp96 in hepatocytes would drastically affect normal physiological

functions. More importantly, such reasoning also positions gp96 as an attractive therapeutic target against hepatocellular carcinoma given the possibility that gp96 loss might lead to severe ER stress and cell death.

A recent study has shown however that conditional deletion of gp96 and *Pten* from mouse livers using *Albumin-Cre* mice increased liver tumorigenesis (17). This was attributed to the hepatocyte loss of surface integrins and cellular adhesion, and expansion of liver progenitor cells. However, the gp96 status of these tumors was not examined, which makes the field ponder if gp96 plays a pro-oncogenic or tumor-suppressive role. This point is important to resolve, because a tumor-suppressive role of gp96 would have been incompatible with the widely reported correlation between over-expression of gp96 in human cancers and poor clinical prognosis (18–20).

Herein, by crossing the same *Albumin-cre* mice used in the recent study (17) with our independently generated gp96-floxed mice (1), we systemically studied the roles of gp96 in liver biology. We found that *albumin-cre* mediated deletion is not 100% efficient. The presence of gp96+ and gp96− hepatocytes in the same host presented to us a unique system to address the liver-intrinsic roles of gp96. We found that the KO mice were more susceptible to hepatocyte carcinogenesis, but the developing tumors were exclusively gp96+, due to a compensatory expansion of the residual WT hepatocytes. Furthermore, we also discovered that an asynchronous gp96 loss was associated with elevated ceramides in KO hepatocytes and appearance of macro/micro-vesicular steatosis in the expanding WT cell population, thus linking liver regeneration with increased sphingolipid biogenesis for the first time. Finally, the pro-survival roles of gp96 were also supported by our findings that genetic and pharmacological inhibition of gp96 in human HCC cell lines significantly abrogated their growth.

Materials and Methods

Mice

Liver-specific gp96 KO mice were generated by crossing *Albumin-cre* mice (21) with *Hsp90b1*$^{flox/flox}$ mice (1, 7, 22) to obtain *Albumin-cre Hsp90b1*$^{flox/flox}$ *mice*. All animals were maintained as per the guidelines of the Institutional Animal Care and Use Committee at the Medical University of South Carolina (MUSC).

Liver function tests

Serum levels of alanine aminotransferase and total bilirubin were measured at the Yale University Mouse Metabolic Phenotypic Center. Serum was collected by bleeding the mice by cardiac puncture and allowing blood to coagulate for 30 minutes at room temperature in the dark to maintain bilirubin stability, followed by centrifugation at 5,000×*g* to remove the pellet.

Immunohistochemistry

Livers were fixed in formalin and dehydrated in 30% sucrose-PBS, then embedded in OCT for subsequent cutting into 5 μm sections using a cryotome, as described (4). For staining,

sections were fixed for 10 minutes by acetone at −20°C, washed with PBS and then permeablized with methanol for 5 minutes at −20°C. Sections were then washed with PBS. The endogenous peroxidase was quenched with 3% H_2O_2 for 5 minutes and blocked with 2% normal goat serum for 2 hours at room temperature. Primary antibodies, such as gp96 antibody (9G10, Stressgen) and Ki67 antibody (NB110-89717, Novus Biologicals), were applied for 1 hour at room temperature, followed by incubation with secondary antibodies and avidin-HRP from the ABC Systems of Vector BioLabs.

Sphingolipid quantification

Sphingolipid levels were measured by the high-performance liquid chromatography/ mass spectrometry (LC-MS/MS) methodology as previously described (23). Analytical results of lipids were expressed as pmol of lipids / total cellular protein (pmol/mg).

MALDI Imaging

MALDI (matrix-assisted laser desorption ionization) imaging was performed as previously described (24). Briefly, MALDI-FTICR imaging mass spectrometry (MALDI-IMS) was utilized for on-tissue detection and spatial localization of ceramides and sphingolipids in liver tissues from gp96 knockout or WT mice. 2, 5-Dihydroxybenzioc Acid (DHB), and trifluoroacetic acid were obtained from Sigma-Aldrich (St. Louis, MO). HPLC-grade methanol, ethanol, and water were obtained from Fisher Scientific. Indium tin oxide (ITO)-coated slides were purchased from Bruker for MALDI-IMS experiments. Whole excised livers were placed in weigh-boats and rapidly frozen with liquid nitrogen in the vapor-phase for 2 minutes and stored at −80 until sectioning. Tissues were sectioned at 14 μm thickness. Samples were mounted on ITO coated slides, and desiccated at room temperature for 20 minutes. An ImagePrep spray station (Bruker Daltonics) was used for addition of Dihydroxybenzoic acid (DHB) matrix at a concentration of 0.2 M in 50% methanol and 0.1% trifluoroacetic acid (TFA). Spectra were acquired in positive mode across the entire tissue section on a Solarix dual source 7T FT-ICR mass spectrometer (Bruker Daltonics) to detect the lipid species of interest (m/z 200–1200) with a SmartBeam II laser operating at 1000 Hz, a laser spot size of 25 μm, and a raster width of 75 μm. For each laser spot, 400 spectra were averaged. Images of differentially expressed lipids were generated using FlexImaging 4.0 software (Bruker Daltonics). Following MS analysis, data was loaded into FlexImaging Software focusing on the m/z range 200–1200 and reduced to 0.99 ICR Reduction Noise thresholds. All data was normalized using root means square.

Myriocin treatment

Inhibition of *de novo* sphingolipid synthesis was done by intra-peritoneal injection of WT and KO mice with the serine-pamitoyl transferase (SPT) inhibitor myriocin, at a dose of 0.3 mg/kg body weight every 48 hours for 16 days (25). Myriocin was dissolved in DMSO and further diluted 10 times in PBS before injecting into mice.

Liver carcinogenesis

Liver tumors were induced by injecting 15 day-old pups with 25 mg/kg diethyl-nitrosoamine (DENA) before weaning or genotyping (26, 27). Mice were followed for 34 weeks until

sacrifice. Tumor quantification was performed by counting grossly visible surface tumor nodules.

Hepatoma cell growth assays

Hepatoma cell lines were tested via MTT assay by plating 6×10^3 cells/well in a 96-well plate and adding 0.5 mg/mL of MTT [3-(4,5-dimethylthiazol-2-yl)-2,5-diphenyltetrazolium bromide] at the designated time points for 3 hours at 37°C. Cells were then dissolved by 100 μL DMSO and absorbance was read at 595 nm. For the carboxyfluorescein succinimidyl ester (CFSE) dilution assay, cells were incubated with 5 μM CFSE in PBS at room temperature for 10 minutes in the dark, followed by washing with complete media and PBS. Where indicated, cells were treated with IL-6 (10 ng/mL), TWS119 (750 nM), LiCl (25 mM), tauroursodeoxycholic acid (TUDCA) (25 μM), 4-phenylbutyric acid (1 mM), IGF-1 (100 ng/mL), myriocin (50 ng/mL) and/or hepatocyte growth factor (HGF) (140 ng/mL). To knockdown gp96, HepG2 cells were transduced with a lentivirus encoding gp96 shRNA or scrambled shRNA (from Open Biosystems), as described previously (20). Starting 2 days after transduction, transduced cells were selected with 2 μg/mL puromycin for 3 days.

Microarray analysis

HepG2 cells were cultured with WS13 (10 μM) for 24 hours and RNA was harvested using RNeasy Plus Mini Kit (Qiagen). cDNA gene expression analysis was performed on a OneArray chip by Phalanx Biotechnologies. Differentially expressed genes were mapped into biological processes using KEGG Pathways and DAVID databases. Heat maps were generated using HeatMapViewer software from Broad Institute.

Statistical Analysis

Two-way ANOVA was used for comparing weight curves. Otherwise, two-tailed *t*-test was used for all other comparisons. Error bars represent standard error of the mean (SEM) unless otherwise specified. *$p<0.05$, **$p<0.01$, ***$p<0.0001$.

Results

Hepatocyte-specific deletion of gp96 results in compromised liver function and nodular steatosis

To study the role of gp96 in liver homeostasis, we crossed *Albumin-Cre* and *Hsp90b1*$^{flox/flox}$ mice to generate *Albumin-Cre Hsp90b1*$^{flox/flox}$ offspring (KO mice) in C57BL/6 background, which demonstrated deletion of gp96 (Hsp90b1) in the liver (Figure 1A). KO mice did not appear grossly abnormal, were fertile and survived for over 12 months. They manifested mild elevation of serum total bilirubin, indicative of a compromised but well-compensated baseline liver function (Figure 1B). The liver in young KO mice was atrophic, weighing around 50% of WT liver weight at 6 weeks (Figure 1C). Curiously, as mice aged, the liver weight of KO mice caught up with that of WT mice, resulting in no significant difference between the two groups at around 1 year of age (Figure 1C). Strikingly, gross examination of KO livers revealed apparent surface fatty nodules ranging between 1 and 2 mm in diameter (Figure 1D) in both male and female mice. Hematoxylin & Eosin staining demonstrated both micro- and macro-vesicular steatotic appearance (Figure 1E). The fat

content of the nodules was confirmed by a positive Oil Red O staining (Figure 1F). There was no significant fibrosis/cirrhosis with the KO livers based on lack of picrosirius red staining (Supplementary Fig. 1A). Baseline analysis also revealed a slight elevation of selective ER stress response genes, including ATF6 and CHOP in both young (3 month old) and old (1 year old) mice (Supplementary Fig. 1B,C). We saw no significant apoptotic cells in the nodule by TUNEL assay (data not shown).

Loss of gp96 in hepatocyte results in age-dependent expansion and steatosis of residual WT hepatocytes

Unexpectedly, immunohistochemical staining for gp96 in KO livers showed the steatotic nodules to be exclusively gp96+ and the adjacent non-steatotic hepatocytes to be devoid of gp96 (gp96−) (Figure 2A). The presence of both gp96+ and gp96− cells in the same livers presented us a unique opportunity to compare the two cellular populations kinetically to determine the intrinsic roles of gp96 in hepatocyte biology. Following those KO mice over time, from 6 weeks till 1 year, we found that gp96+ cells were enriched with age: <5% at 6 weeks, 42% at 3 months and 90% at 1 year (Figure 1B). Moreover, staining for Ki67 in 3 month old mouse livers demonstrated higher proliferative rates in gp96+ nodules compared to adjacent gp96− hepatocytes in KO mice or normal hepatocytes from WT mice (Figures 1C and D), indicating that the remaining gp96+ cells in the KO livers are under pro-proliferative pressure resulting in higher Ki67 expression and enrichment with age. Thus, in the absence of gp96, hepatocytes suffered from significant growth disadvantage which allowed a small number of hepatocytes with unsuccessful cre-mediated gp96 deletion to take over the entire organ. The rapid expansion of these WT cells did have metabolic consequences as they were found to have a striking steatotic picture with significant accumulation of lipids intracellularly.

Derangement of sphingolipid metabolism in the livers of the KO mice

Bioactive sphingolipids play important roles in regulating cell survival and death (28). For examples, there is a link between the role of glycoceramides and hepatic steatosis in *ob/ob* mice fed with high-fat diet (29, 30). Ceramide accumulation has also been implicated in alcohol-related steatohepatitis (31, 32). We thus turned our attention to the possible beneficial roles of sphingolipids that contribute to both the nodular steatosis and the expansion of residual gp96+ cells in the liver of KO mice. We utilized a MALDI imaging technique to quantify sphingolipid level in liver tissue sections *in situ*, which allowed us to simultaneously examine the structure of the liver parenchyma. Strikingly, the KO livers contain higher levels of sphingolipids including C18 ceramide and sphingosine-1-phosphate (Sph-1P) than WT counterparts, which was especially more prominent in the fatty nodules in the KO livers (Figure 3).

We next quantified the levels of ceramides and Sph-1P in the liver lysates by mass spectrometry. As expected, KO livers contained significantly higher levels of multiple long chain ceramide entities compared to the WT livers (Figure 4A). In addition, a quantitative PCR mini-array of genes for 40 sphingolipid metabolic enzymes showed selective enzymes to be up-regulated in KO livers at the mRNA level, including ceramide synthase 1 (Cers1), alkaline ceramidase 1 (Acer1), sphingomyelin phophodiesterase 5 (Smpd5) and serine-

palmytoyl transferase (SPT) LC3 (Sptlc3) (Figure 4B). Ceramides are potent inducers of cellular apoptosis, and multiple mediators have been shown to propagate this pro-apoptotic effect, including ceramide activated protein kinase (CAPK) (33), cathepsin D (34) and protein phosphatases 1 and 2A (PP1 and PP2A) (35, 36). The accumulation of ceramides in KO liver and the elimination of gp96− cells as the mice age suggest that the higher ceramide levels in KO cells contribute to their demise with time.

Next, we tested the possibility that *de novo* ceramide synthesis plays a role in the accumulation of fat in the adjacent gp96+ nodules. Two-month-old female mice were injected with the SPT-specific inhibitor myriocin every 48 hours for 16 days, to block the rate-limiting step of *de novo* ceramide synthesis. Indeed, myriocin treatment resulted in a significant reduction in the number of surface steatotic nodules (Figure 4C). However, blocking ceramide synthesis with myriocin resulted in hepatocyte injury as shown by a 3-fold elevation in serum ALT levels (Figure 4D), compromised hepatocyte function evidenced by > 8-fold increase in total bilirubin (Figure 4E) and reduced liver mass (Figure 4F). Taken together, our data support two important principles in the roles of sphingolipids in hepatocyte biology. First, gp96 negatively regulates the biogenesis of long chain ceramides which is a part of an adaptive process to overcome their survival disadvantage in the case of ongoing ceramide overload. Second, *de novo* sphingolipid biosynthesis can either directly or indirectly predispose hepatocytes to undergo steatotic changes.

Liver-specific knockout of gp96 increases the tumorigenicity of adjacent gp96+ hepatocytes

A recent study demonstrated that conditional deletion of gp96 and *Pten* from mouse livers using *Albumin-Cre* mice increased liver tumorigenesis (17). However, cDNA microarray analysis of gp96 expression in cancer and adjacent normal tissue from a publicly available dataset (37, 38) showed over-expression of gp96 in hepatocellular carcinoma (Figure 5A). Moreover, increased expressions of gp96 in multiple cancer types have been reported to correlate with poorer prognosis (18–20). We next decided to definitely determine whether gp96 is an oncogenic chaperone or a tumor suppressor, using a well-established liver carcinogenesis model. Fifteen-day-old male and female pups were injected with the carcinogen diethyl-nitrosoamine (DENA) intraperitoneally and monitored for 34 weeks until sacrifice. At this time point, all male mice were expected to develop liver tumors ranging from microcarcinoma to visible lesions (27). KO mice displayed an increased number of surface tumors, and a bigger tumor burden (Number of nodules × average nodular size) (Figures 5B and 5C). All of the WT males developed tumors, but with an average of only 4.5 tumors/mouse, compared to 27 tumors/mouse in KO males ($p<0.005$). As for the females, only 1 out of 6 WT females developed a tumor, compared to 11 of 11 KO females. The average tumor number was 0.167 tumors/mouse in WT females compared to 6 tumors/mouse in KO females ($p<0.001$). This demonstrates a strong predisposition for tumorigenesis in KO mice. Consistent with the increased susceptibility to cancer in KO mice, each of KO males and females showed less gain of body weight than WT males and females, respectively ($p<0.05$) (Figure 5D) and more elevation in serum ALT, indicative of more severe cancer-associated hepatocyte injury (Figure 5E). Importantly, both WT and KO

tumors were positive for albumin by immunofluorescent stain, consistent with the hepatic origin of the cancers (Supplementary Figure 2).

Strikingly however, although KO mice were more susceptible to DENA-induced tumors, their tumors were almost exclusively gp96+ (Figure 5F). This is consistent with our observation that gp96− cells are at a survival disadvantage. Given that the gp96+ cells in KO mice have higher proliferation rates at baseline; this could render them more susceptible to mutations and subsequent transformation, resulting in the gp96+ tumors being more prevalent in KO livers. The mere proliferative drive of WT cells in the KO livers could by itself result in a bigger tumor toll as well, without necessarily accumulating more mutations. This proliferative drive in the gp96+ cells in KO livers is reflected by the increased levels of hepatocyte growth factor (HGF) in adjacent non-cancerous tissue (Figure 5G). Importantly, HGF is not elevated in KO livers at 6 weeks of age, when the vast majority of hepatocytes are still gp96− (Figure 5H).

gp96 is indispensable for hepatoma cell growth and is a promising therapeutic target against hepatocellular carcinoma

Given the survival disadvantage of gp96-deficient cells in KO mice at baseline and upon cancer induction, we reasoned that targeted inhibition of gp96 in established hepatocellular carcinoma (HCC) would be detrimental for those cells. Therefore, two human HCC cell lines, HepG2 and PLC, were treated with a purine scaffold-based selective inhibitor of ATP-binding and ATPase activity of gp96, WS13 (20), for 5 days. Inhibition of gp96 resulted in significant attenuation in the expansion of both cell types by a MTT assay (Figures 6A and 6B). Further analysis of HepG2 cells after 3 days of treatment with WS13 showed a significant reduction in the Wnt signaling pathway, reflected by lower levels of total β-catenin and its downstream target cyclin D1 (Figure 6C). WS13-treated cells also expressed lower levels of HGF, accompanied by a reduction in the levels of cell growth signals including p-ERK1/2, p-AKT and p-STAT3, which are some of the key downstream targets of HGF (Figure 6C). As a readout for ER stress, qRT-PCR was performed on WS13-treated cells which showed moderate elevation of expression of genes in the unfolded protein response pathway, including ATF4 and CHO (Supplementary Figure 3).

Autophagy is an adaptive cellular mechanism essential for cellular survival at baseline and under stress conditions. We found that inhibition of gp96 in HepG2 cells resulted in the reduction of beclin1, indicating a compromise in the auto-phagocytic function of those cells. Full-length PARP, which is involved in DNA repair, is also decreased upon gp96 inhibition, which correlates with the cellular commitment to death, where severely damaged cells stop DNA repair machinery and commit to the apoptotic pathway. gp96 inhibition in PLC cells also resulted in the down-regulation of β-catenin, PARP and Beclin1 (Figure 6C), while HGF and its downstream signaling molecules were already minimally expressed at baseline.

Consistent with our pharmacological data, knocking down (KD) gp96 from HepG2 cells by shRNA lentiviral transduction resulted in a significant attenuation of cellular division, as evidenced by the minimal CFSE dilution at day 3 (Figure 6D). This was associated with increased levels of cell death, shown by propidium iodide staining (Figure 6E). Therefore, loss of gp96 function in hepatoma cell lines results in the reduction of cellular division and

rise in cell death, leading to the overall attenuation of cell expansion. In addition, gp96 KD HepG2 cells were inert to the stimulation by HGF which had no effect on cellular division, whereas HGF treatment of scrambled shRNA-transduced cells further promoted cellular proliferation (Figure 6D). To determine whether any of the defective Wnt signaling or ER homeostasis pathways played a role in this phenomenon, WS13-treated or gp96 knockdown hepatoma cells were treated with the GSK3β inhibitors TWS119 and LiCl (20), and chemical chaperones tauroursodeoxycholate (TUDCA) and 4-phenyl butyric acid (PBA) (39). None of those interventions or their combination was sufficient to rescue the hepatoma cell growth. Given the roles of IL-6, IGF-1 and HGF in hepatocyte regeneration and hepatoma cellular survival (40), we also attempted but were unable to rescue the growth defect of WS13-treated and/or gp96 KD hepatoma cells by supplying these molecules exogenously (Supplementary Fig. 4). Collectively, we conclude that gp96 regulates hepatocyte biology via multiple pathways.

Concordant with the ceramide changes seen *in vivo*, WS13-treated HepG2 hepatoma cells accumulated different species of d18 and d16 ceramides, mostly in the long chain and very long chain ranges (Figure 6F,G). In parallel, PLC and HepG2 cell lines demonstrated up-regulation of SPTLC1, SPTLC2 and/or SPTLC3, 3 enzyme subunits involved in the rate-limiting step of *de novo* ceramide synthesis (Figure 6H, I). To determine the early events occurring in hepatoma cells after gp96 inhibition and that could contribute to their growth arrest, HepG2 cells were treated with the gp96 inhibitor WS13 (10 μM) for 24 hours, and their gene expression profile was analyzed using a whole genome human cDNA microarray. Inhibition of gp96 resulted in the up-regulation of 148 genes and down-regulation of 59. The up-regulated genes were most highly enriched for metabolism-related ones such as cytochrome P450 enzymes and those involved in organic acid catabolism (ACSM5, ACSS2, SAT2 and BDH1) (Figure 6J). More importantly, nine of the down-regulated genes were involved in cell cycle, eight of which take part in the mitotic phase in particular (Figure 6K), which potentially explains the growth arrest observed in gp96 KD and WS13-treated cells.

Discussion

gp96 plays a pivotal role in cellular physiology, due to its role in metabolic stress (41), ER quality control (9), calcium homeostasis (42), IGF production and signaling (43), Wnt pathway (4) and others. It is up-regulated in liver diseases where significant metabolic pressure and cellular proliferation are present, including hepatocellular carcinoma, liver cirrhosis and hepatitis B viral infection (44). Therefore, loss of gp96 function, whether in normal physiological conditions or in disease, is expected to incur a huge toll on the cellular well-being, especially in highly synthetic and metabolically active cells such as hepatocytes and cancer cells.

Herein, we performed hepatocyte-specific deletion of gp96 by crossing *hsp90b1*$^{flox/flox}$ mice with *Alb-cre* mice. Our strategy was efficient, as we achieved more than 95% deletion of gp96 in ~6 week old KO mice, analyzed by immunohistochemistry (Fig. 2B). However, cre-mediated recombination was not 100% faithful leaving out a small but definitive percentage of residual hepatocytes to retain gp96 expression. Due to this asynchronous deletion of gp96 in hepatocytes in our model, we were able to discern the hepatocyte-intrinsic roles of gp96

in the baseline hepatic function as well as during the hepatic carcinogenesis. Remarkably, we found gp96 deletion in hepatocytes positioned them at a tremendous growth disadvantage in that the percentage of gp96− hepatocytes in the KO mice decreased from over 95% in young mice (~6 weeks old) to less than 5% when mice reached 1 year old. During this period of adaptation, a variety of novel metabolic disarrangements were uncovered which shed significant light on the roles of gp96 in hepatic steatosis and cancer (Figure 7). First, regenerating gp96+ hepatocytes underwent remarkable steatotic changes, which raises an intriguing possibility of increasing metabolic demand to the liver as the underlying uniform mechanism for all other non-alcoholic steatohepatitis. Second, the abrogation of gp96 by both genetic and pharmacological means was associated with an elevation of long chain ceramides, and upregulation of a number of enzymes in the biogenesis of ceramides. This finding suggests that gp96 plays previously unrecognized roles in maintaining sphingolipid homeostasis. Further studies of the underlying mechanisms may prove to be fruitful, particularly related to the possibility of gp96 in regulating key enzymes in the sphingolipid biogenesis and catabolism, as well as the emerging cross-talk between sphingolipid biology and unfolded protein response. Importantly, ceramide accumulation in gp96− cells and gp96+ cells in the KO liver was shown to contribute to hepatic steatosis in gp96+ cells, suggesting paracrine signaling via sphingolipids as an important mechanism for nodular steatohepatitis. Third, regenerating gp96+ hepatocytes were more predisposed to carcinogenesis, which was associated with increased production of HGF from the surrounding tissues (Fig. 5G). Persistent signaling from HGF through its receptor c-MET is known to promote hepatocellular carcinoma (45).

Our genetic study demonstrates that gp96 is required for *de novo* hepatic oncogenesis which took more than 6 months to develop. Acute inhibition of gp96 either pharmacologically or genetically was also shown to be effective against hepatic cancers (Figure 6). The underlying mechanisms most likely are multi-factorial given the fact that gp96 is an obligated chaperone for a variety of key signaling pathways such as Wnt (4), integrin (3, 6) and insulin-like growth factor (5, 46), besides its roles as an important effector molecules in the unfolded protein response pathway (10, 11). Not surprisingly, activating any one of these pathways alone was unable to rescue cell death in response to pharmacological inhibition of gp96.

Our study has significant implications in the pathogenesis of hepatic steatosis and neoplasms in general. It suggests that there is a common denominator for the two processes: i.e. liver regeneration. We propose that chronic underlying liver injuries of viral, metabolic, alcoholic, drug-induced or any other etiologies will result in a compensatory liver regenerative process, which if continues in a protracted period of time becomes a driving force for steatosis and regenerative neoplasms. Many of the studies in the field are consistent with this model (47–53).

A recent study also demonstrated that hepatocyte deletion of gp96 in *Albumin-Cre HSP90b1*$^{flox/flox}$ mice promoted oncogenesis in response to *Pten* genetic deletion from hepatocytes, which was attributed to the expansion of liver progenitor cells (17). In the current work, we observed a similar phenomenon of increased tumorigenisis in the KO mice in response to a chemical carcinogen. The status of gp96 expression in PTEN-loss tumor

was not reported (17), whereas in our carcinogenesis model, almost all of the tumors developed in the KO background were nonetheless gp96+. The development of gp96+ tumors but not gp96− tumors in the same mice allowed us to conclude that gp96 plays an intrinsically tumor-promoting role in hepatocellular carcinoma. Our findings are also consistent with multiple previous studies demonstrating that liver-specific knockout of pro-tumorigenic genes including another ER chaperone grp78 could result in paradoxical enhancement of tumorigenesis, where the tumors arose from cells that have escaped cre-mediated deletion of the target gene (47, 54, 55).

Altogether, our study demonstrated that gp96 is an oncogenic chaperone in hepatocyte carcinogenesis. The clinical relevance of our study is many-fold, not the least of which is the significant over-expression of gp96 in hepatocellular carcinoma and the availability of gp96− selective inhibitor. Due to the roles of gp96 in chaperoning multiple strategically important oncogenic clienteles such as integrin, Wnt co-receptor, IGF1 and TLR, gp96-targeted therapy may prove to be a promising therapeutic modality for liver cancer.

Supplementary Material

Refer to Web version on PubMed Central for supplementary material.

Acknowledgements

We thank all the past and present members in Z. Li's laboratory for their support and stimulating discussion during the course of the study. Z. Li is the Abney Chair Remembering Sally Abney Rose in Stem Cell Biology & Therapy, and is supported by the SmartState Endowed Chair Program of South Carolina, USA.

Financial support: This study was supported in part by NIH grants AI070603, AI077283 (to Z.L.), CA97132 (to Y.A.H.), and a VA Merit Award 2I0BX000200-04 (to A.C.). It was also supported by the Lipidomics Shared Resource, Hollings Cancer Center, Medical University of South Carolina (P30 CA138313) and the Lipidomics Core in the SC Lipidomics and Pathobiology COBRE, Department of Biochemistry and Molecular Biology, MUSC (P20 RR017677).

Abbreviations

DENA	diethyl-nitrosoamine
ER	endoplasmic reticulum
HCC	hepatocellular carcinoma

References

1. Yang Y, Liu B, Dai J, Srivastava PK, Zammit DJ, Lefrancois L, Li Z. Heat shock protein gp96 is a master chaperone for toll-like receptors and is important in the innate function of macrophages. Immunity. 2007; 26:215–226. [PubMed: 17275357]
2. Liu B, Yang Y, Qiu Z, Staron M, Hong F, Li Y, Wu S, et al. Folding of Toll-like receptors by the HSP90 paralogue gp96 requires a substrate-specific cochaperone. Nat Commun. 2010; 1:79. [PubMed: 20865800]
3. Wu S, Hong F, Gewirth D, Guo B, Liu B, Li Z. The molecular chaperone gp96/GRP94 interacts with Toll-like receptors and integrins via its C-terminal hydrophobic domain. J Biol Chem. 2012; 287:6735–6742. [PubMed: 22223641]

4. Liu B, Staron M, Hong F, Wu BX, Sun S, Morales C, Crosson CE, et al. Essential roles of grp94 in gut homeostasis via chaperoning canonical Wnt pathway. Proc Natl Acad Sci U S A. 2013; 110:6877–6882. [PubMed: 23572575]
5. Barton ER, Park S, James JK, Makarewich CA, Philippou A, Eletto D, Lei H, et al. Deletion of muscle GRP94 impairs both muscle and body growth by inhibiting local IGF production. FASEB J. 2012; 26:3691–3702. [PubMed: 22649033]
6. Liu B, Li Z. Endoplasmic reticulum HSP90b1 (gp96, grp94) optimizes B-cell function via chaperoning integrin and TLR but not immunoglobulin. Blood. 2008; 112:1223–1230. [PubMed: 18509083]
7. Staron M, Yang Y, Liu B, Li J, Shen Y, Zuniga-Pflucker JC, Aguila HL, et al. gp96, an endoplasmic reticulum master chaperone for integrins and Toll-like receptors, selectively regulates early T and B lymphopoiesis. Blood. 2010; 115:2380–2390. [PubMed: 19965672]
8. Hong F, Liu B, Chiosis G, Gewirth DT, Li Z. alpha7 Helix Region of alphaI Domain Is Crucial for Integrin Binding to Endoplasmic Reticulum Chaperone gp96: A POTENTIAL THERAPEUTIC TARGET FOR CANCER METASTASIS. J Biol Chem. 2013; 288:18243–18248. [PubMed: 23671277]
9. Kozutsumi Y, Segal M, Normington K, Gething MJ, Sambrook J. The presence of malfolded proteins in the endoplasmic reticulum signals the induction of glucose-regulated proteins. Nature. 1988; 332:462–464. [PubMed: 3352747]
10. Yang Y, Li Z. Roles of heat shock protein gp96 in the ER quality control: redundant or unique function? Mol Cells. 2005; 20:173–182. [PubMed: 16267390]
11. Lee AS. Glucose-regulated proteins in cancer: molecular mechanisms and therapeutic potential. Nat Rev Cancer. 2014; 14:263–276. [PubMed: 24658275]
12. Malhotra JD, Kaufman RJ. The endoplasmic reticulum and the unfolded protein response. Semin Cell Dev Biol. 2007; 18:716–731. [PubMed: 18023214]
13. Walter P, Ron D. The unfolded protein response: from stress pathway to homeostatic regulation. Science. 2011; 334:1081–1086. [PubMed: 22116877]
14. Korennykh A, Walter P. Structural basis of the unfolded protein response. Annu Rev Cell Dev Biol. 2012; 28:251–277. [PubMed: 23057742]
15. Tabas I, Ron D. Integrating the mechanisms of apoptosis induced by endoplasmic reticulum stress. Nat Cell Biol. 2011; 13:184–190. [PubMed: 21364565]
16. Gardner BM, Pincus D, Gotthardt K, Gallagher CM, Walter P. Endoplasmic reticulum stress sensing in the unfolded protein response. Cold Spring Harb Perspect Biol. 2013; 5:a013169. [PubMed: 23388626]
17. Chen WT, Tseng CC, Pfaffenbach K, Kanel G, Luo B, Stiles BL, Lee AS. Liver-specific knockout of GRP94 in mice disrupts cell adhesion, activates liver progenitor cells, and accelerates liver tumorigenesis. Hepatology. 2014; 59:947–957. [PubMed: 24027047]
18. Wang XP, Wang QX, Ying XP. Correlation between clinicopathology and expression of heat shock protein 72 and glycoprotein 96 in human gastric adenocarcinoma. Tohoku J Exp Med. 2007; 212:35–41. [PubMed: 17464101]
19. Wang X, Wang Q, Lin H. Correlation between clinicopathology and expression of heat shock protein 72 and glycoprotein 96 in human esophageal squamous cell carcinoma. Clin Dev Immunol. 2010; 2010:212537. [PubMed: 20300187]
20. Hua Y, White-Gilbertson S, Kellner J, Rachidi S, Usmani SZ, Chiosis G, Depinho R, et al. Molecular Chaperone gp96 Is a Novel Therapeutic Target of Multiple Myeloma. Clin Cancer Res. 2013; 19:6242–6251. [PubMed: 24077352]
21. Postic C, Shiota M, Niswender KD, Jetton TL, Chen Y, Moates JM, Shelton KD, et al. Dual roles for glucokinase in glucose homeostasis as determined by liver and pancreatic beta cell-specific gene knock-outs using Cre recombinase. J Biol Chem. 1999; 274:305–315. [PubMed: 9867845]
22. Staron M, Wu S, Feng H, Stojanovic A, Du X, Bona R, Liu B, et al. Heat shock protein gp96 chaperones platelet glycoprotein Ib-IX-V complex and protects mice from Bernard-Soulier syndrome-like platelet disorder. Blood. 2011; 117:7136–7144. [PubMed: 21576699]

23. Bielawski J, Pierce JS, Snider J, Rembiesa B, Szulc ZM, Bielawska A. Sphingolipid analysis by high performance liquid chromatography-tandem mass spectrometry (HPLC-MS/MS). Adv Exp Med Biol. 2010; 688:46–59. [PubMed: 20919645]
24. Jones EE, Powers TW, Neely BA, Cazares LH, Troyer DA, Parker AS, Drake RR. MALDI imaging mass spectrometry profiling of proteins and lipids in clear cell renal cell carcinoma. Proteomics. 2014; 14:924–935. [PubMed: 24497498]
25. Russo SB, Baicu CF, Van Laer A, Geng T, Kasiganesan H, Zile MR, Cowart LA. Ceramide synthase 5 mediates lipid-induced autophagy and hypertrophy in cardiomyocytes. J Clin Invest. 2012; 122:3919–3930. [PubMed: 23023704]
26. Lu S, Archer MC. Insulin-like growth factor binding protein-1 over-expression in transgenic mice inhibits hepatic preneoplasia. Mol Carcinog. 2003; 36:142–146. [PubMed: 12619036]
27. Koen H, Pugh TD, Goldfarb S. Hepatocarcinogenesis in the mouse. Combined morphologic-stereologic studies. Am J Pathol. 1983; 112:89–100. [PubMed: 6190407]
28. Hannun YA, Obeid LM. Principles of bioactive lipid signalling: lessons from sphingolipids. Nat Rev Mol Cell Biol. 2008; 9:139–150. [PubMed: 18216770]
29. Bijl N, Sokolovic M, Vrins C, Langeveld M, Moerland PD, Ottenhoff R, van Roomen CP, et al. Modulation of glycosphingolipid metabolism significantly improves hepatic insulin sensitivity and reverses hepatic steatosis in mice. Hepatology. 2009; 50:1431–1441. [PubMed: 19731235]
30. Zhao H, Przybylska M, Wu IH, Zhang J, Maniatis P, Pacheco J, Piepenhagen P, et al. Inhibiting glycosphingolipid synthesis ameliorates hepatic steatosis in obese mice. Hepatology. 2009; 50:85–93. [PubMed: 19444873]
31. Tong M, Longato L, Ramirez T, Zabala V, Wands JR, de la Monte SM. Therapeutic reversal of chronic alcohol-related steatohepatitis with the ceramide inhibitor myriocin. Int J Exp Pathol. 2014; 95:49–63. [PubMed: 24456332]
32. Fernandez A, Matias N, Fucho R, Ribas V, Von Montfort C, Nuno N, Baulies A, et al. ASMase is required for chronic alcohol induced hepatic endoplasmic reticulum stress and mitochondrial cholesterol loading. J Hepatol. 2013; 59:805–813. [PubMed: 23707365]
33. Muller G, Ayoub M, Storz P, Rennecke J, Fabbro D, Pfizenmaier K. PKC zeta is a molecular switch in signal transduction of TNF-alpha, bifunctionally regulated by ceramide and arachidonic acid. EMBO J. 1995; 14:1961–1969. [PubMed: 7744003]
34. Heinrich M, Wickel M, Winoto-Morbach S, Schneider-Brachert W, Weber T, Brunner J, Saftig P, et al. Ceramide as an activator lipid of cathepsin D. Adv Exp Med Biol. 2000; 477:305–315. [PubMed: 10849758]
35. Wolff RA, Dobrowsky RT, Bielawska A, Obeid LM, Hannun YA. Role of ceramide-activated protein phosphatase in ceramide-mediated signal transduction. J Biol Chem. 1994; 269:19605–19609. [PubMed: 8034729]
36. Dobrowsky RT, Kamibayashi C, Mumby MC, Hannun YA. Ceramide activates heterotrimeric protein phosphatase 2A. J Biol Chem. 1993; 268:15523–15530. [PubMed: 8393446]
37. Roessler S, Jia HL, Budhu A, Forgues M, Ye QH, Lee JS, Thorgeirsson SS, et al. A unique metastasis gene signature enables prediction of tumor relapse in early-stage hepatocellular carcinoma patients. Cancer Res. 2010; 70:10202–10212. [PubMed: 21159642]
38. Roessler S, Long EL, Budhu A, Chen Y, Zhao X, Ji J, Walker R, et al. Integrative genomic identification of genes on 8p associated with hepatocellular carcinoma progression and patient survival. Gastroenterology. 2012; 142:957–966. e912. [PubMed: 22202459]
39. Ozcan U, Yilmaz E, Ozcan L, Furuhashi M, Vaillancourt E, Smith RO, Gorgun CZ, et al. Chemical chaperones reduce ER stress and restore glucose homeostasis in a mouse model of type 2 diabetes. Science. 2006; 313:1137–1140. [PubMed: 16931765]
40. Michalopoulos GK, DeFrances MC. Liver regeneration. Science. 1997; 276:60–66. [PubMed: 9082986]
41. Shiu RP, Pouyssegur J, Pastan I. Glucose depletion accounts for the induction of two transformation-sensitive membrane proteinsin Rous sarcoma virus-transformed chick embryo fibroblasts. Proc Natl Acad Sci U S A. 1977; 74:3840–3844. [PubMed: 198809]
42. Van PN, Peter F, Soling HD. Four intracisternal calcium-binding glycoproteins from rat liver microsomes with high affinity for calcium. No indication for calsequestrin-like proteins in inositol

1,4,5-trisphosphate-sensitive calcium sequestering rat liver vesicles. J Biol Chem. 1989; 264:17494–17501. [PubMed: 2793869]

43. Radosevic-Stasic B, Jakovac H, Grebic D, Trobonjaca Z, Mrakovcic-Sutic I, Cuk M. Heat shock protein Gp96 as potential regulator of morphostasis after partial hepatectomy in mice. Curr Aging Sci. 2012; 5:254–262. [PubMed: 23387888]
44. Zhu XD, Li CL, Lang ZW, Gao GF, Tien P. Significant correlation between expression level of HSP gp96 and progression of hepatitis B virus induced diseases. World J Gastroenterol. 2004; 10:1141–1145. [PubMed: 15069714]
45. Goyal L, Muzumdar MD, Zhu AX. Targeting the HGF/c-MET pathway in hepatocellular carcinoma. Clin Cancer Res. 2013; 19:2310–2318. [PubMed: 23388504]
46. Wanderling S, Simen BB, Ostrovsky O, Ahmed NT, Vogen SM, Gidalevitz T, Argon Y. GRP94 is essential for mesoderm induction and muscle development because it regulates insulin-like growth factor secretion. Mol Biol Cell. 2007; 18:3764–3775. [PubMed: 17634284]
47. Chen WT, Zhu G, Pfaffenbach K, Kanel G, Stiles B, Lee AS. GRP78 as a regulator of liver steatosis and cancer progression mediated by loss of the tumor suppressor PTEN. Oncogene. 2013
48. Zhang K, Wang S, Malhotra J, Hassler JR, Back SH, Wang G, Chang L, et al. The unfolded protein response transducer IRE1alpha prevents ER stress-induced hepatic steatosis. EMBO J. 2011; 30:1357–1375. [PubMed: 21407177]
49. Adinolfi LE, Gambardella M, Andreana A, Tripodi MF, Utili R, Ruggiero G. Steatosis accelerates the progression of liver damage of chronic hepatitis C patients and correlates with specific HCV genotype and visceral obesity. Hepatology. 2001; 33:1358–1364. [PubMed: 11391523]
50. Browning JD, Horton JD. Molecular mediators of hepatic steatosis and liver injury. J Clin Invest. 2004; 114:147–152. [PubMed: 15254578]
51. Farrell GC, Larter CZ. Nonalcoholic fatty liver disease: from steatosis to cirrhosis. Hepatology. 2006; 43:S99–S112. [PubMed: 16447287]
52. Seitz HK, Stickel F. Molecular mechanisms of alcohol-mediated carcinogenesis. Nat Rev Cancer. 2007; 7:599–612. [PubMed: 17646865]
53. El-Serag HB, Rudolph KL. Hepatocellular carcinoma: epidemiology and molecular carcinogenesis. Gastroenterology. 2007; 132:2557–2576. [PubMed: 17570226]
54. Thompson MD, Wickline ED, Bowen WB, Lu A, Singh S, Misse A, Monga SP. Spontaneous repopulation of beta-catenin null livers with beta-catenin-positive hepatocytes after chronic murine liver injury. Hepatology. 2011; 54:1333–1343. [PubMed: 21721031]
55. Sekine S, Ogawa R, Kanai Y. Hepatomas with activating Ctnnb1 mutations in 'Ctnnb1-deficient' livers: a tricky aspect of a conditional knockout mouse model. Carcinogenesis. 2011; 32:622–628. [PubMed: 21216847]

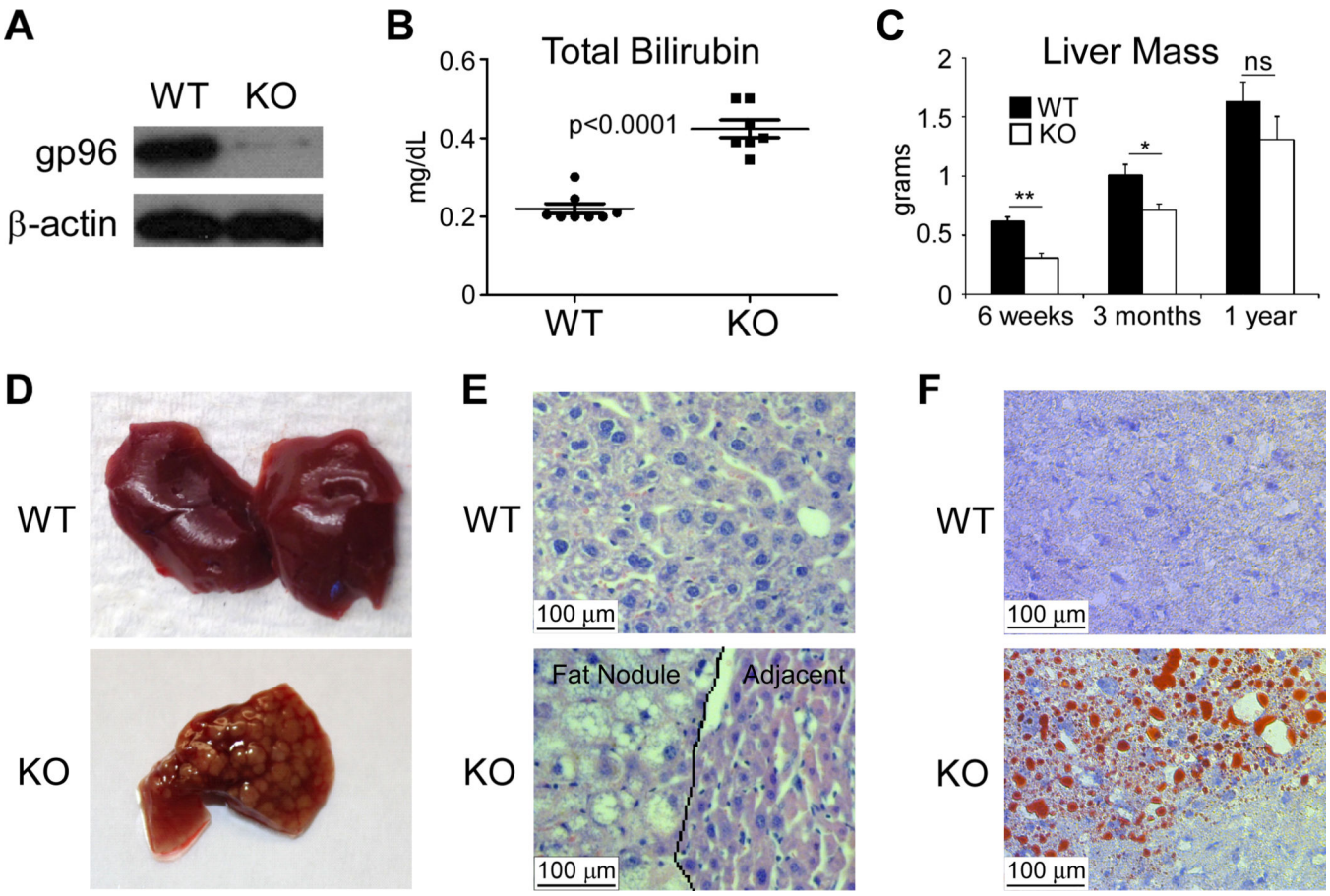

Figure 1. Atrophy, poor function and focal steatosis of livers in mice with liver-specific gp96 deletion

(**A**) Immunoblot for gp96 in the whole hepatic lysates of 6 week-old, WT and liver-specific gp96 KO mice (WT, n=3; KO, n=4). (**B**) Total bilirubin in the serum of 3 month-old mice (WT, n=8; KO n=7). (**C**) Masses of livers from WT and KO mice at different ages (6 weeks: 3 WT and 3 KO. 3 months: 5 WT and 5 KO. 1 year: 6 WT and 7 KO). (**D**) Gross appearance of WT and KO livers (Representative of >10 mice). (**E**) H&E staining of liver section of 3 month-old mice (Representative of 5 mice per group). The margin between steatotic lesion and normal appearing hepatocyte regions was indicted. (**F**) Oil red O staining of hepatic section from WT and KO mice (Representative of 5 mice per group). * $p<0.05$, ** $p<0.01$, ns: non-significant by 2-tailed student t-test.

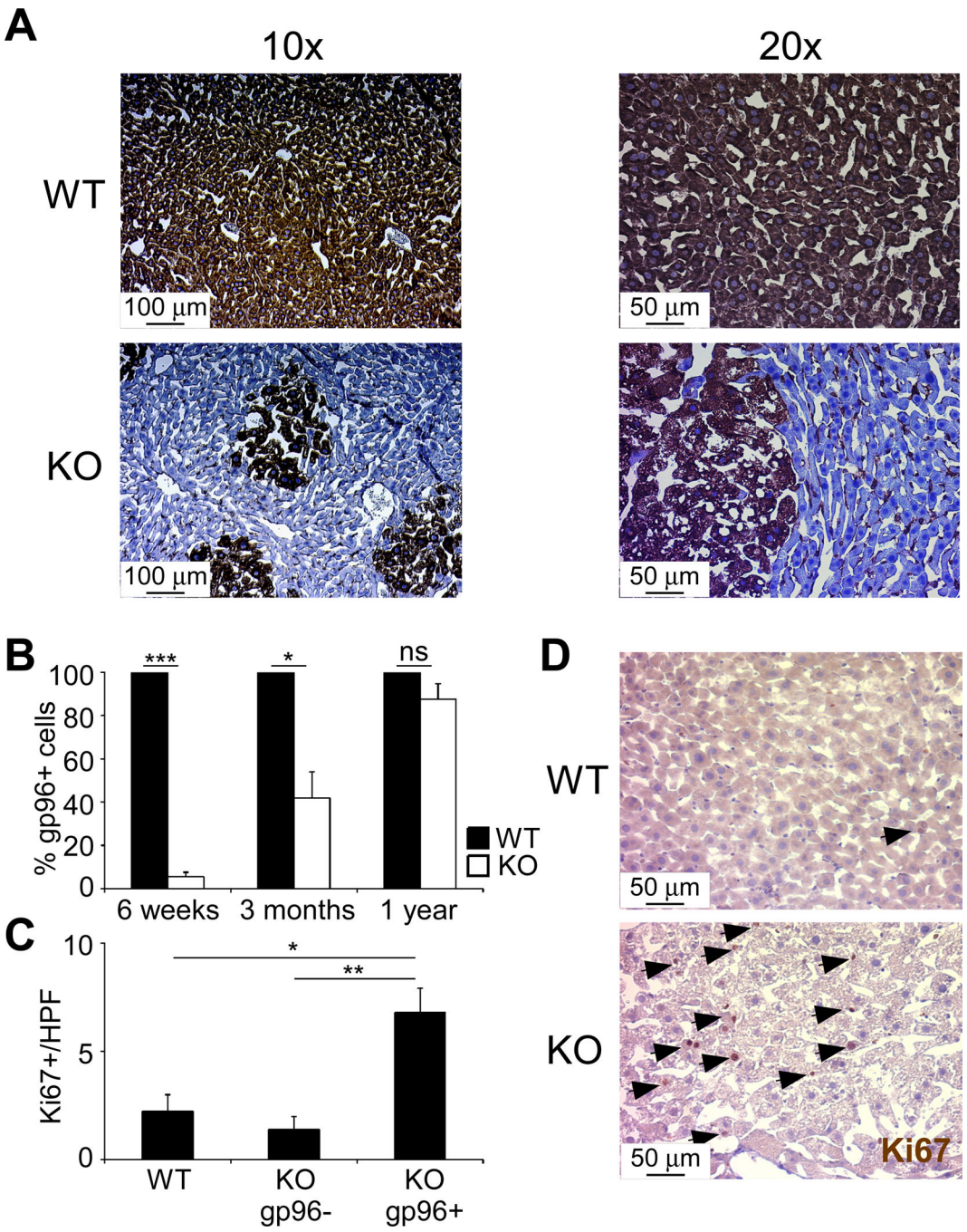

Figure 2. gp96-KO livers contain residual gp96+ cells that expand with age

(**A**) Immunohistochemical staining of gp96 on the liver sections from WT and KO mice. (**B**) Quantification of gp96+ hepatocytes with age (n=5/group). (**C**) Quantification of Ki67+ cells per high power field in the livers of 3 month-old mice (n=5/group). (**D**) Immunohistochemical staining Ki67 as in (**C**) (n=5/group). Arrows indicate Ki67+ cells. * p<0.05, ** p<0.01, *** p<0.0001, ns: non-significant by 2-tailed student t-test.

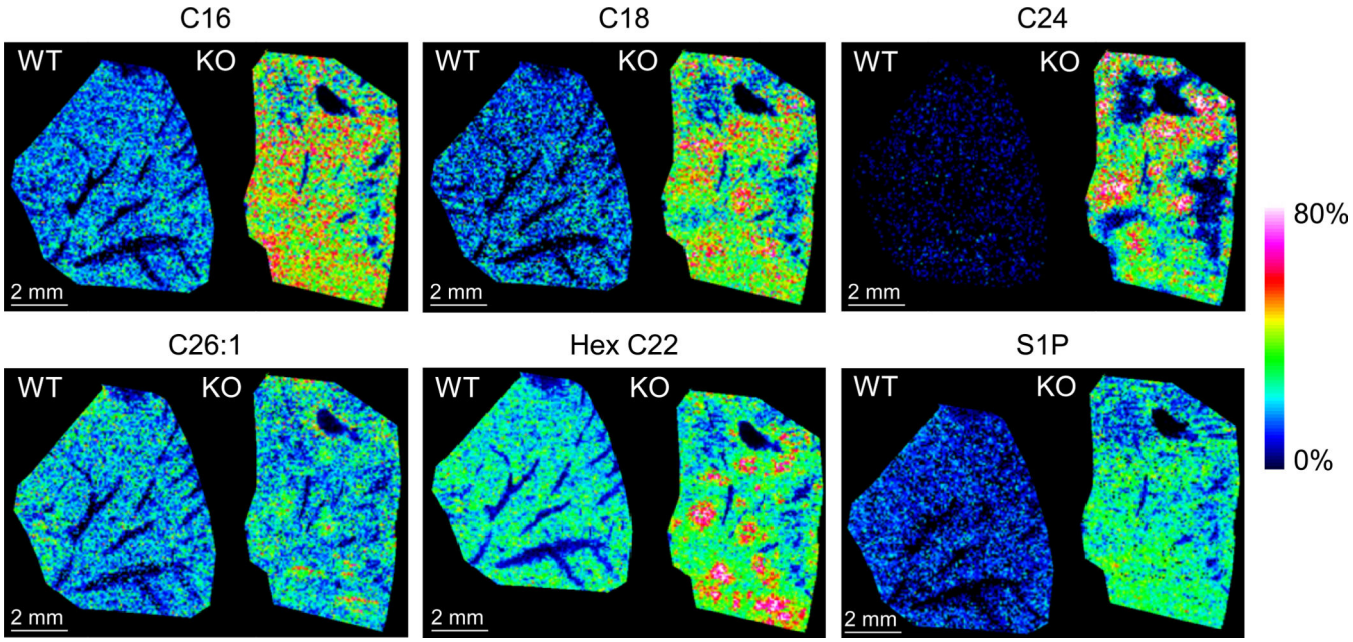

Figure 3. Elevation of sphingolipids in KO livers, particularly in gp96+ nodules

MALDI imaging was performed on WT and KO liver sections to visualize tissue distribution of ceramides and S1P using mass spectrometry. Color intensity represents abundance of molecules measured.

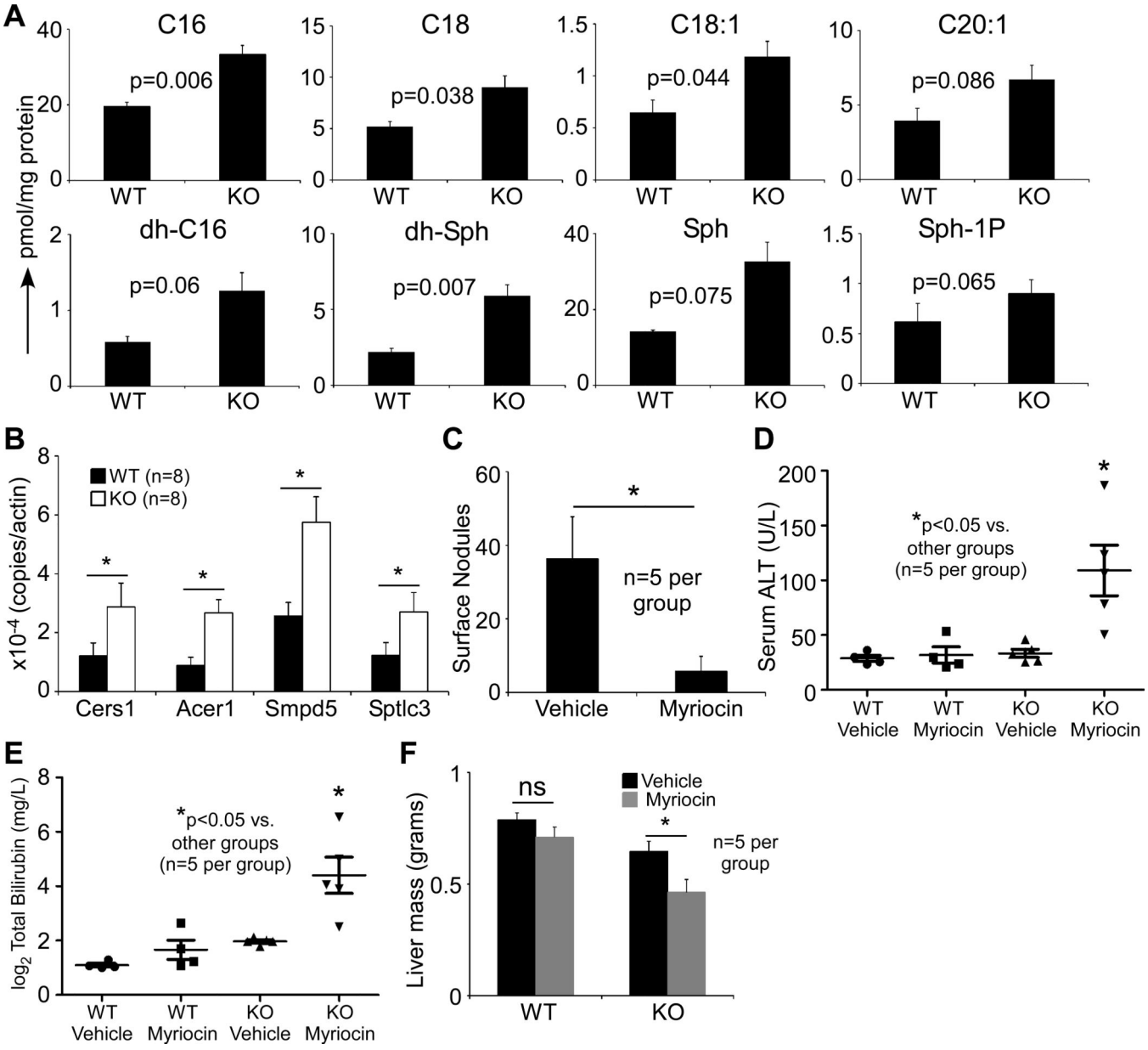

Figure 4. Ceramide entities are accumulated in gp96-KO cells and contribute to the compensated liver function

(**A**) Mass spectrometry-based quantification of ceramides and S1P levels in 3 WT and 4 KO livers. (**B**) qRT-PCR of mRNA level of four sphingolipid metabolizing enzymes in 3 month-old livers, including ceramide synthase 1 (Cers1), alkaline ceramidase 1 (Acer1), sphingomyelin phosphodiesterase 5 (Smpd5) and serine-palmytoyl transferase long chain subunit 3 (Sptlc3) (n=8 per group). (**C**) Number of surface steatotic hepatic nodules in response to myriocin treatment in 2 month-old mice (n=5 per group). (**D–F**) Serum ALT levels (**D**), total bilirubin (**E**) and liver mass (**F**) in untreated and myriocin-treated WT and KO mice (n=5 per group). * p<0.05, ns: non-significant by 2-tailed student t-test.

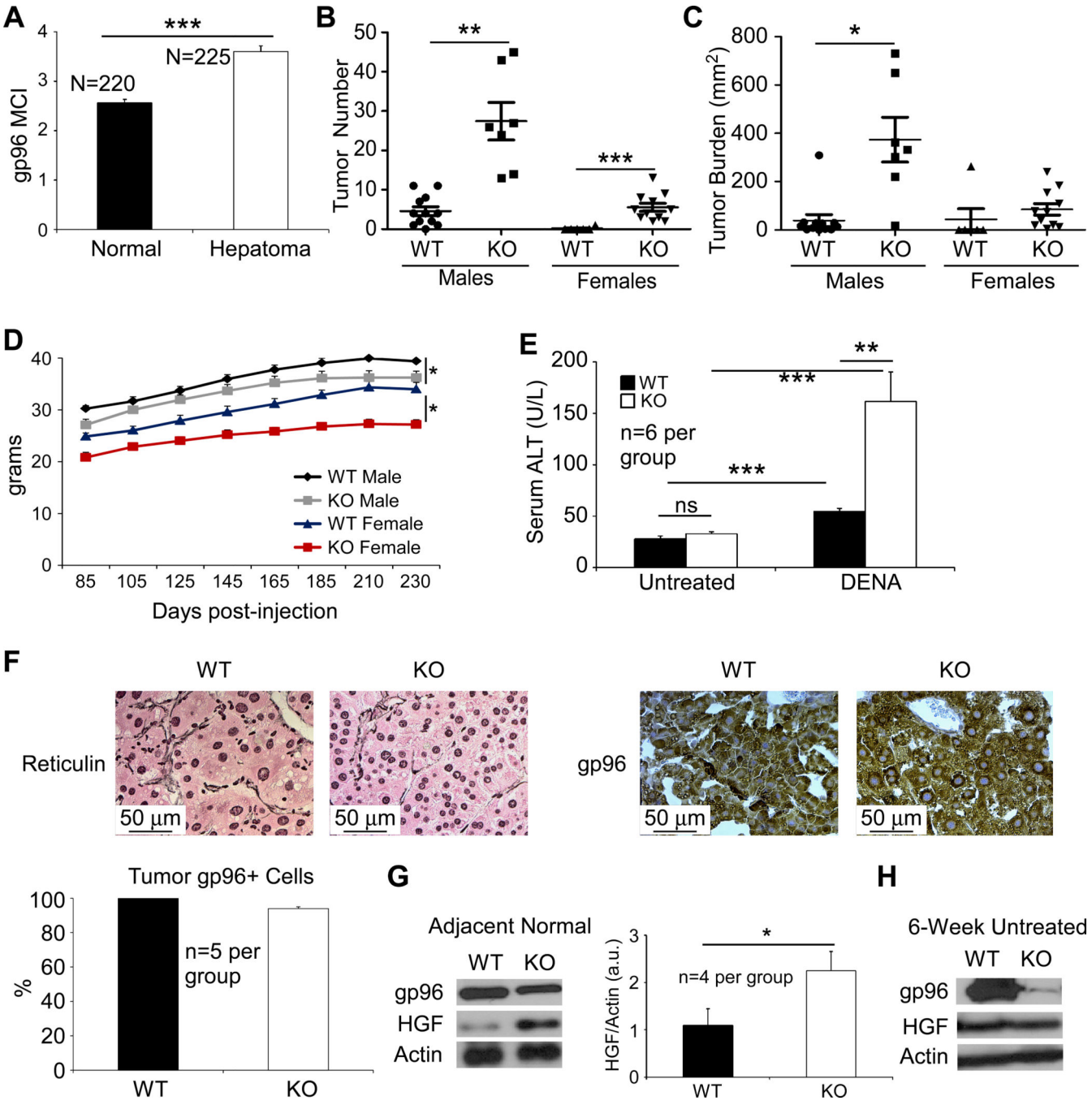

Figure 5. Residual gp96+ hepatocytes in the liver-specific gp96 KO mice are highly susceptible to chemical carcinogenesis

(**A**) cDNA microarray analysis shows mRNA levels of gp96 in human hepatocellular carcinoma. (**B,C**) Surface tumors (**B**) and tumor burden (**C**) in diethylnitrosamine (DENA)-treated mice 32 weeks post-injection (WT males, n=12; KO males, n=7; WT females, n=6; KO females, n=11). (**D**) Post-DENA weight curve in mice of both sexes described in (B). (**E**) Serum ALT levels in untreated and tumor-bearing mice (n=6 per group). (**F**) Reticulin and gp96 stains of DENA-induced tumors, and quantification of gp96+ cells in tumors from

WT and KO mice (n=5 per group). (**G**) Immunoblot of HGF in adjacent normal tissue of WT and KO livers at 32 weeks post induction (n=4 per group). (**H**) HGF expression in untreated WT and KO mice at 6 weeks of age, when the KO liver is mostly gp96− (n=4 per group). * $p<0.05$, ** $p<0.01$, *** $p<0.0001$, ns: non-significant by 2-tailed student t-test.

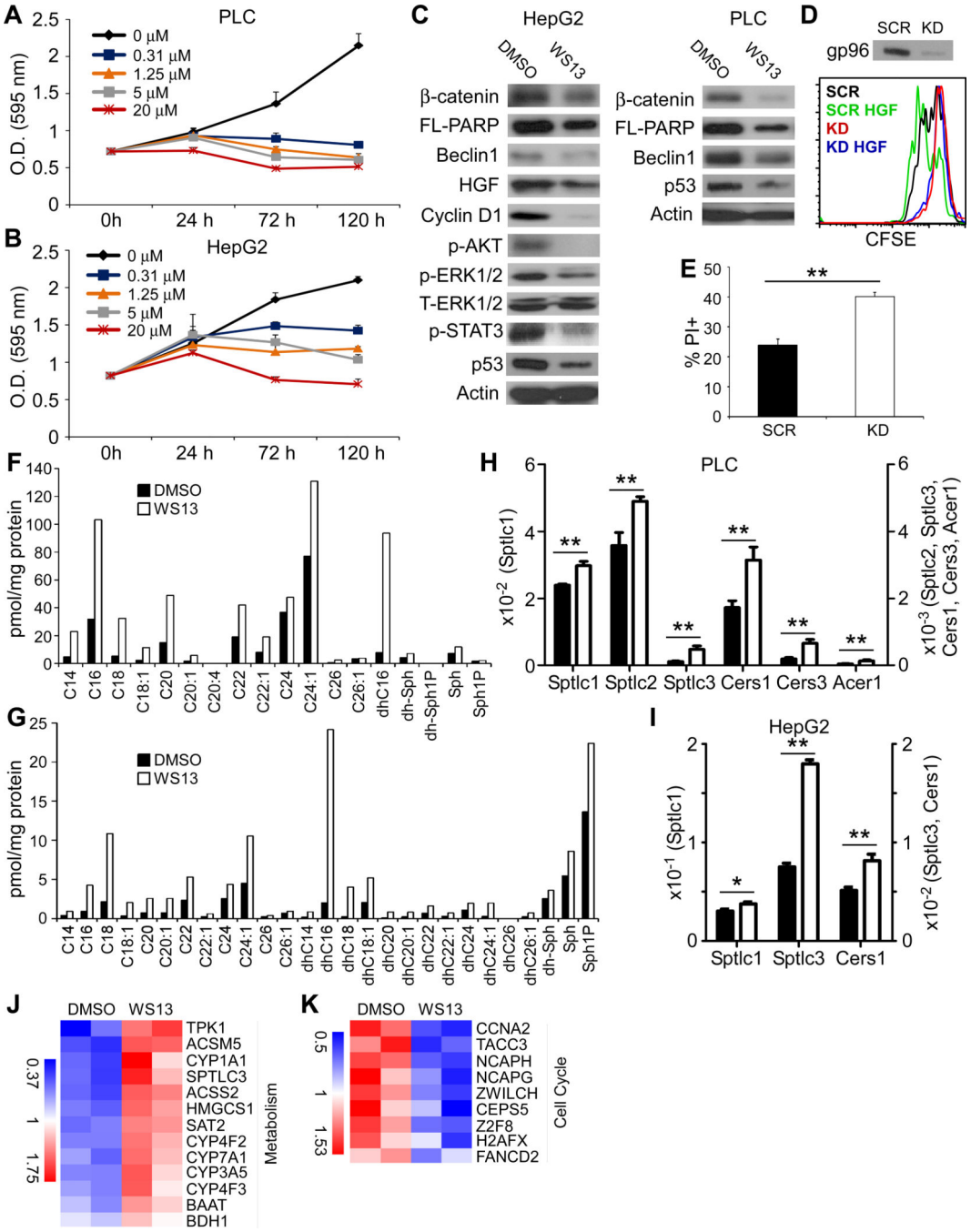

Figure 6. Targeting gp96 in human hepatoma cell lines abrogates their growth capacity and induces ceramide accumulation

(**A,B**) HepG2 (**A**) and PLC (**B**) HCC cells were treated with different doses of WS13 for 5 days, followed by MTT assay (representative of 2 experiments). (**C**) Immunoblot for β-catenin, PARP, Beclin1, HGF, Cyclin D1, p-AKT, p-ERK1/2, and p-STAT3 in hepatoma cells after 3 days of treatment with WS13 (representative of 2 experiments). (**D**) Cellular proliferation quantified by CFSE dilution in gp96 knockdown and control cells, with or without recombinant human HGF treatment. (**E**) Quantification of cell death by propidium

iodide nuclear staining. (**F,G**) d18 (**F**) and d16 (**G**) base ceramides in HepG2 cells treated with WS13 (10 μM) for 3 days. (**H,I**) qRT-PCR of ceramide-generating enzymes and alkaline ceramidase in PLC and HepG2 cells treated with 2 μM (PLC) or 6 μM (HepG2) WS13 for 36 hours. Error bars in (**H**) and (**I**) represent standard deviation. (**J,K**) HepG2 cells were treated with WS13 (10 μM) for 24 hours and RNA was harvested for cDNA gene expression analysis. * $p<0.05$, ** $p<0.01$, ns: non-significant by 2-tailed student t-test.

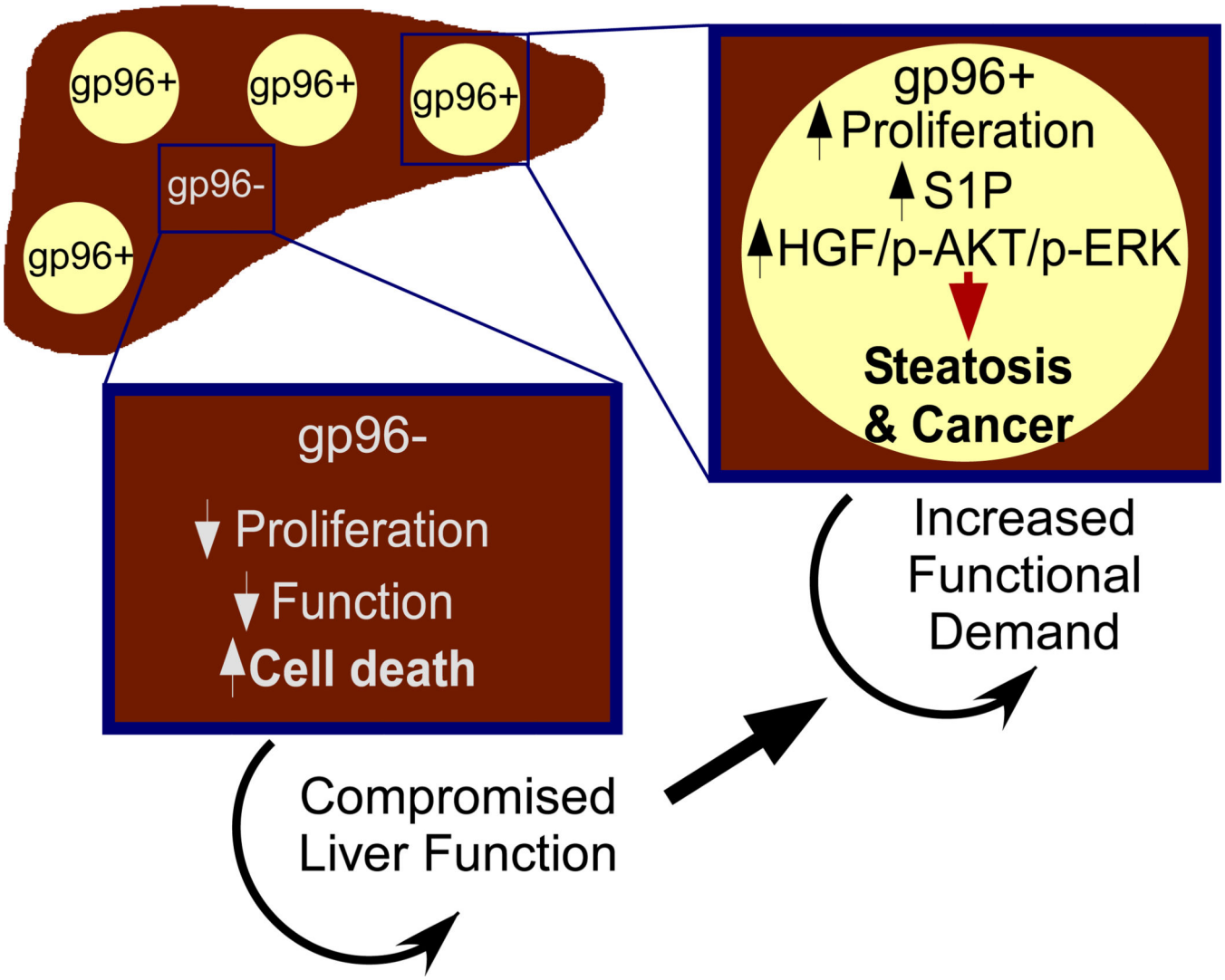

Figure 7. A schematic model of the roles of gp96 in hepatocyte biology and cancer

The asynchronous deletion of gp96 in this study uncovered that gp96 promotes hepatic steatosis and oncogenesis via empowering cell proliferation and survival via multiple pathways including sphingolipid biosynthesis.